Journal of Environmental Management 275 (2020) 111266

Contents lists available at ScienceDirect

Journal of Environmental Management

journal homepage: http://www.elsevier.com/locate/jenvman

Research article

Staged electrochemical treatment guided by modelling allows for targeted recovery of metals and rare earth elements from acid mine drainage

Emma Thompson Brewster [a,b], Stefano Freguia [c], Mansour Edraki [b], Luke Berry [c], Pablo Ledezma [c,*]

[a] Kinetic Group Worldwide Pty Ltd, University of the Sunshine Coast, 90 Sippy Downs Drive, Sippy Downs, QLD, 4556, Australia
[b] Centre for Mined Land Rehabilitation, Sustainable Minerals Institute, The University of Queensland, St Lucia, QLD, 4072, Australia
[c] Advanced Water Management Centre, The University of Queensland, St Lucia, QLD, 4072, Australia

ARTICLE INFO

Keywords:
Electrochemical treatment
Acid mine drainage
Neutralisation
Resource recovery
Rare earth elements

ABSTRACT

Acid mine drainage (AMD) is a challenge for current and legacy mining operations worldwide given its potential to severely harm ecosystems and communities if inadequately managed. Treatment costs for AMD are amongst the highest in the industrial wastewater treatment sector, with limited sustainable options available to date. This work demonstrates a novel chemical-free approach to tackle AMD, whereby staged electrochemical neutralisation is employed to treat AMD and concomitantly recover metals as precipitates. This approach was guided by physico-chemical modelling and tested on real AMD from two different legacy mine sites in Australia, and compared against conventional chemical-dosing-based techniques using hydrated lime ($Ca(OH)_2$) and sodium hydroxide (NaOH). The electrochemical treatment demonstrated the same capacity than $Ca(OH)_2$ to neutralise AMD and remove sulfates, and both were significantly better than NaOH. However, the electrochemical approach produced less voluminous and more easily settleable sludge than $Ca(OH)_2$. Moreover, the staged treatment approach demonstrated the potential to produce metal-rich powdered solids with a targeted composition, including rare earth elements and yttrium (REY). REY were recovered in concentrations up to 0.1% of the total solids composition, illustrating a new avenue for AMD remediation coupled with the recovery of critical metals.

1. Introduction

Acid mine drainage, or acid rock drainage (hereafter referred to collectively as AMD), is a major global environmental issue with limited economically-viable options for safe and sustainable prevention or remediation (Simate and Ndlovu, 2014). Treatment options are largely limited by costs due to transport requirements, large volumes of secondary waste (sludge), high electricity and chemical needs, and lack of locally-available resources (e.g. grid energy and operational personnel) (Rakotonimaro et al., 2016; Wang et al., 2018).

AMD forms when rocks, usually containing pyrite (FeS_2), are exposed to oxygen, water and/or oxidising microorganisms, resulting in oxidation processes that dissolve the iron and other elements present in the rock (Fernando et al., 2018). The resulting contaminated water is often acidic and contains high concentrations of sulfate, iron and other transition, heavy metals, and metalloids of toxic significance (Kefeni et al., 2017). The primary methods of AMD treatment applied at industrial scale globally use the basic principle of neutralisation by *e.g.* adding alkaline chemicals (NaOH, lime, limestone, etc.), chemical oxidants for iron removal (e.g. H_2O_2) and/or microorganisms (for a comprehensive review of AMD treatment options, see reviews by Akcil and Koldas (2006) and Kefeni et al. (2017)). This (bio)chemical neutralisation results in increased solution pH and the precipitation of metal (oxy)hydroxides and sulfates (Thompson-Brewster et al., 2018; Thompson Brewster et al., 2016). The solubility theory of these processes and the resulting precipitates is well understood and a variety of modelling platforms are available to simulate neutralisation experiments. These models include: *i)* the evaluation of ion pairing and acid-base reactions using laws of mass-action, *ii)* ionic strength using chemical activity correction factors, *iii)* pH using a charge and/or mass balance, and *iv)* saturation using a saturation index (SI)(Morel et al., 1993; Stumm and Morgan, 2013). However, one of the key limitations of conventional (bio)chemical neutralisation is the production of large volumes of precipitate sludge that requires dewatering and safe

---

* Corresponding author.
E-mail address: p.ledezma@awmc.uq.edu.au (P. Ledezma).

https://doi.org/10.1016/j.jenvman.2020.111266
Received 9 April 2020; Received in revised form 10 August 2020; Accepted 17 August 2020

disposal/storage, which combined with treatment and transport costs, can make site management prohibitively expensive (Rakotonimaro et al., 2016). Electrolytic technologies are considered an interesting alternative to the above given that the only consumable supply required is the low-cost commodity electricity and that they can treat AMD to similar standards by removing metals by (co)precipitation and sulfate by ionic migration (when an anion-exchange membrane is used in the configuration) (Chartrand and Bunce, 2003). Known advantages of the electrochemical *vs* the chemical-dosing approach are the lower volumes of sludge produced that are easier to dewater; the production of sulfuric acid as an exportable by-product (recognisably of very-low value) and the co-precipitation of most AMD metals in a controllable manner, meaning these could be potentially recovered (Bejan and Bunce, 2015). Known disadvantages however include the fouling of membranes/electrodes when the (co)precipitates coat the active surfaces required for the process, a lack of clarity as to how these processes can be successfully upscaled for industrial-scale use and the relatively higher capital expenditure (CAPEX) required – as electrochemical reactors are typically more expensive than almost all other wastewater treatment technologies on the market (Strathmann, 2004).

As for conventional wastewater treatment, a circular economy approach to AMD treatment requires concomitant resource recovery, which in this case can furthermore help offset the inherent high CAPEX of electrochemical treatment (Fernando et al., 2018; Naidu et al., 2019). Targets for recovery from AMD include metals and metalloids, sulfur products (e.g. elemental sulfur, sulfuric acid), electrical energy, construction materials (e.g. gypsum), agricultural soil conditioners or adsorbents (Naidu et al., 2019; Nleya et al., 2016; Pozo et al., 2017; Simate and Ndlovu, 2014).

A further product of special interest are higher-value rare earth elements and yttrium (REY)(Naidu et al., 2019). REY are required for clean energy generation, rechargeable batteries, photovoltaic cells, fibre optics and lasers, and their demand is expected to grow significantly in the near future (Alonso et al., 2012; Arshi et al., 2018; Browne et al., 2019). There already are anticipated issues with the accelerated growth of REY consumption due to unsustainable mining, monopolistic supply conditions and potential geopolitical conflicts (Alonso et al., 2012; Browne et al., 2019). These problems could however be alleviated by substitution, security-of-supply policies and finding alternative REY sources, such as recovery from AMD treatment (Arshi et al., 2018; Barnhart and Benson, 2013).

In this work, we propose the use of electrochemical treatment for pH neutralisation of AMD as an alternative to (bio)chemical neutralisation. We demonstrate that this electrochemical approach does not require chemical additions to treat AMD and facilitates the recovery of metals and REY. The approach and evaluation of this electrochemical system for treatment with concomitant targeted recovery of metals was guided by first-principles-based physico-chemical modelling through controlling the pH at several stages, corresponding to stages identified in the model. The proposed method was furthermore directly compared to conventional chemical neutralisation approaches using NaOH and lime, both through modelling and experimental demonstration.

2. Methods

2.1. Modelling methods

Metal solubility theory dictates that different metals oxides, hydroxides and sulfates become saturated at different pH values. Modelling of the major precipitants was performed, which involved removing sulfate (as would happen in the electrochemical treatment) or adding lime or NaOH (as would happen during chemical addition treatment).

Simulations using PHREEQC (Version 3) were performed to understand saturation and precipitation of high concentration metals during the different experiments in the cathodic reservoir of the electrochemical experiments and a single reservoir for the chemical addition experiments. The initial solution compositions in PHREEQC were defined based on Inductively Coupled Plasma – Optical Emission Spectrometry (ICP-OES) analysis performed to characterise the real AMD samples (see **2.2.3.**). The components included: Al, Ca, Cu, Fe(II), Fe (III), Mg, Mn, Na, SO_4^{2-} and Zn, as they were in relatively high concentrations ($>$0.8 mM) and were present in the database used (WATEQ4F) (Parkhurst et al., 2013).

The formation of equilibrium phases (solids and gas) were modelled using the EQUILIBRIUM_PHASES block in PHREEQC (Parkhurst et al., 2013). The specific equilibrium phases included in the model were determined by running a simulation with the EQUILIBRIUM_BLOCK included, but no phases listed as forming to identify the possible mineral phases above saturation (considered conservatively to be a saturation index greater than 0). Thereafter, a second simulation including all the potential mineral phases previously identified in the simulation described above was performed to evaluate which ones actually formed according to the model. Non-forming mineral phases were removed from subsequent simulations. A list of all equilibrium phases included in the simulations can be found in the electronic supplementary information (ESI) Table S1.

Simulations were performed to match the laboratory experiments described in Section 2.2. To model the AMD in the cathode section of the electrochemical experiments, sulfate was removed stepwise. For the chemical experiments, NaOH or CaO was added stepwise using a REACTION block (Parkhurst et al., 2013). The resulting mineral-phase and aqueous concentrations after sulfate removal or chemical addition are the model output. There are two key limitations to the modelling: a) the PHREEQC database in use (WATEQ4F) is limited to certain components and precipitation products and b) low concentration metals ($<$0.8 mM) were not included due to simulations crashing when including them as components, possibly due to tolerance issues when solving for both high and low concentration components simultaneously.

2.2. Experimental methods

2.2.1. Overview

Two types of experiments were performed using the system configuration presented in Fig. S1. The first type of experiment consisted of three treatments comparing the efficacy and sludge quality of electrochemical AMD treatment and chemical dosing with NaOH and slaked lime. These experiments were performed in two pH stages (hereafter referred to as two-stage experiments; see Section 2.2.5). The first stage elevated the pH to 4.2 and the second to 10.2. After each stage, several types of settling tests were performed.

The second type of experiments were multistage tests (see Section 2.2.6) using only the electrochemical reactor (Fig. S1). These multistage tests increased the pH in smaller increments of 0.5 or 1 units, which provided refined data on the nature of the precipitation relating to pH. No chemical treatment was performed for the multistage tests.

2.2.2. Electrochemical reactor setup

The electrochemical system used here was designed to demonstrate the potential for metal recovery and AMD treatment at a laboratory scale. It followed the principle that by applying a current between the cathode and anode, the electrochemical reactions increase the pH of the cathodic solution, decrease the pH of anolyte solution and cause anions (in this case sulfate ions) to migrate from the cathode chamber to the anode chamber through an AEM (anion-exchange membrane). The increase in pH of the cathodic solution will concomitantly drive the precipitation of metal (oxy)hydroxides and sulfates.

For both types of experiments the electrochemical reactor consisted of two custom-made acrylic chambers separated by rubber gaskets, a 4 cm by 4 cm mesh stainless steel cathode, a 4 cm by 4 cm mesh platinum-iridium oxide coated titanium electrode anode (Magneto Special Anodes B V, Netherlands), and an AEM (Membranes International IC., USA, AEM-7001) with effective surface area of 32 cm^2. Both chambers were 8 cm high, 4 cm wide and 1.2 cm thick (38.4 cm^3). A pump (Watson Marlow Sci 323) was used to supply the electrolytes at a flow rate 85 mL min^{-1} (90 RPM) through the reactor with anolyte and catholyte individually recirculated to external reservoirs (see Fig. S1). The reservoirs were vented to maintain atmospheric pressure.

The anolyte in all experiments was a sodium borate buffer solution was made from 61.83 g boric acid (Sigma-Aldrich, ReagentPlus®≥99.5%, CAS-No: 10043-35-3) and 10 g sodium hydroxide added into 1600 mL MilliQ water, stirred and made up to 2 L with MilliQ water. A strong buffer solution was required in the laboratory experiments as they were run in a batch configuration. A pilot or full-scale system would be run continuously and the anolyte would be producing sulfuric acid solution. For safety reasons (the prevention of very low pH acids) and practical reasons (the prevention of proton leakage across the AEM) for these batch laboratory scale experiments sodium borate buffer was used as it is a strong buffer and relatively inert.

An external power source (Elektro-Automatik GmbH & Co. KG, EA-PS 3016-10B) was used to supply electricity in constant current mode, at current densities in a range between 50 and 200 A m^{-2} (normalised to aforementioned electrode surface area of 32 cm^2) based on experimental verification that these current levels were not limiting (data not shown) and guided by our extensive experience in operating and modelling the behaviour of electrochemical processes treating acid mine drainage and other industrial wastewaters (Ledezma et al., 2019; Pozo et al., 2017; Thompson-Brewster et al., 2018; Thompson Brewster et al., 2017; Thompson Brewster et al., 2016; Ward et al., 2018). During the multi-stage tests the current was kept constant at 0.3 A (93.75 A m^{-2}), the voltage varied between 5.2 and 9.8 V. During the two-stage tests the current and voltage both varied with the voltage between 6.4 and 9.3 V and the current between 0.2 and 0.6 A (62.5–187.4 A m^{-2}). The pH was measured using an Endress + Hauser system (Orbisint CPS11D glass electrode, connected to a Liquisys M DAQ box).

2.2.3. *Acid mine drainage*

In the electrochemical treatments, the catholyte was real AMD collected from the field at two separate locations (unfiltered, but settled, stored < 4 °C until 24 h prior to experiments). Both sources were from legacy sites in Queensland, Australia, and in both sites the AMD generated posed a major environmental risk. One container of AMD was sampled from a tailings pond at each site. They were chemically analysed using ICP-OES and Inductively Coupled Plasma – Mass Spectrometry (ICP-MS) as described in Section 2.2.4, with partial results in Table 1, and full results in ESI Tables S2 and S3.

Site 1 is the Mount Morgan gold mine, which was in operational in Queensland, Australia during the 19th and early 20th century, with approximately 134 million tonnes of waste rock and tailings generated (DNRME, 2018). Mt Morgan gold mine AMD (hereafter Site 1) was found to have remarkably high concentrations of sulfate (29 g L^{-1}), Al (2.3 g L^{-1}), Mg (4.6 g L^{-1}) and Mn (2.4 g L^{-1}), with a pH of 2.7.

The second site of AMD collection has been de-identified. This AMD was collected from a mining operation for a different precious metal and located in a different region of Queensland, Australia. This site (hereafter Site 2) was found to have high concentrations of Al (0.4 g L^{-1}), Fe (0.3 g L^{-1}) and Mg (0.7 g L^{-1}) with a lower sulfate concentration of 9.4 g L^{-1} and similar pH of 2.7, compared to Site 1. The full ICP-OES and ICP-MS analyses of the field collected AMD means there is no reduction in scientific merit of this chemical study even though the sample site has been de-identified.

2.2.4. *Analytical methods*

For the liquid analysis, the composition of the AMD was analysed by inductively coupled plasma optical emission spectroscopy (ICP-OES) for major metals and inductively coupled plasma mass spectrometry (ICP-MS) for trace metals prior to use, with results for the initial composition shown in ESI Tables S2 and S3. ICP-MS samples were unfiltered and digestion was performed using standard methods (USEPA SW846-3005, nitric/hydrochloric acid digestion). The process followed APHA 3125; USEPA SW846 – 6020 and was performed at Analytical Laboratory Services (ALS), Brisbane, Australia. Trace Hg was also analysed for using flow injection mercury system (FIMS) following AS 3550, APHA 3112 Hg-B, which was performed at the same laboratory.

ICP-OES of the liquid samples during experiments was conducted at the Analytical Services Laboratory, The University of Queensland, Brisbane, Australia (PerkinElmer Optima 7300DV, Waltham, MA, USA) after nitric acid digestion for total and soluble cation concentrations. For the dried precipitation products, ICP-OES and ICP-MS analyses were performed at Queensland University of Technology's Central Analytical Research Facility (CARF) using a PerkinElmer Optima 8300 DV Inductively Coupled Plasma Optical Emission Spectrometer and Agilent 8800 Inductively Coupled Plasma Mass Spectrometer, respectively. Methods

Table 1

Treated water quality, a comparison of electrochemically treated (ECR), sodium hydroxide chemical dosing (NaOH) and lime dosing (lime) from ICP-OES analysis in mg L^{-1}. Shaded values are higher than at least one of the guidelines.

Element (mg L^{-1})	Site 1				Site 2				ANZECC 2000 guidelines	
	Original	ECR	NaOH	Lime	Original	ECR	NaOH	Lime	Stock water[a]	Recreational purposes[b]
Al	2317	0.6	0.03	0.7	443	0.6	0.3	5.1	5	0.2
B	0	2.7[c]	0	0	0.7	0.8	0.6	0.6	5	1
Cd	0.1	0	0	0	0.1	0	0	0	0.01	0.005
Ca	364	234	354	442	368	367	377	489	1000	Not listed
Cr	0.02	0	0	0	0.3	0	0	0	1	0.05
Co	5.2	0	0.01	0.06	3	0.01	0.05	0.02	1	Not listed
Cu	65	0.03	0.05	0.07	9	0.2	0.5	0.4	0.4	1
Fe	66	0	0	0	324	0.3	0	0.09	Not sufficiently toxic	0.3
Pb	6.2	0.1	0.07	0.1	1.3	0.01	0.06	0.05	0.1	0.05
Mg	4564	1022	2148	1188	715	318	245	7.4	2000	Not listed
Mn	245	0.8	0.2	0.2	63.4	0.9	0.7	0.1	Not sufficiently toxic	0.1
Ni	2.1	0	0	0	4.7	0.01	0	0	1	0.1
Zn	55	0	0	0	106	0.3	0.03	0.1	20	5
SO_4–S	29 547	4962	27 938	5769	9391	4195	8597	3099	1000	400

[a] ANZECC (2000) Table 4.3.2 also includes the following elements, which were not detectable by ICP-OES analysis: arsenic (Site 2 initially over limit), beryllium (both within limit initially), fluoride (not measured by ICP-MS), mercury (both within limit initially), molybdenum (both within limit initially), selenium (both over limit initially), uranium (both within limit initially), and vanadium (not listed for stock water).

[b] ANZECC (2000) Table 5.2.3 also includes the elements, which were not detectable by ICP-OES analysis: arsenic (both initially over), beryllium (not listed), fluoride (not measured by ICP-MS), mercury (both within limit initially), molybdenum (not listed), selenium (both over limit initially), uranium (not listed), and vanadium (not listed).

[c] Boron increase due to the experimental choice of anolyte (sodium borate) and will not be present during continuous operation.

for analysing the solids bulk composition can be found in the ESI Text S1.

2.2.5. Two-stage tests

Two-stage tests used 1 L of AMD as the catholyte and 1 L of sodium borate buffer solution as the anolyte. The anolyte was replaced as needed when buffer capacity was exhausted and the anolyte pH fell below 7. The catholyte was not replenished. Stage 1 operated until the pH of the AMD (catholyte) reached 4.2. Once the solution reached pH 4.2, the current was turned off. A 20 mL sample was collected for total suspended solids (TSS) analysis. The AMD then underwent a settling rate test (SRT). The SRT was performed by pouring the total AMD (catholyte) solution into a 1 L measuring cylinder. The sludge height was recorded every 3 min for the first 30 min then every 30 min for the next 2 h and finally at 24 h (Pozo et al., 2017). After the settling rate test, a 10 mL sample of the liquid fraction was taken for ICP-OES analysis and the remaining liquid fraction was decanted back into a suitable bottle for the next stage of electrochemical treatment. The sludge volume index was determined by the volume in mL occupied by 1 g of a suspension after 30 min of settling, see Equation (1) below (van Loosdrecht et al., 2016).

$$SVI\ \left(mL\ \ g^{-1}\right) = \frac{settled\ \ sludge\ \ volume\ \ at\ \ 30\ \ min\ \ \left(mL\ \ L^{-1}\right)*1000}{total\ \ suspended\ \ solids\ \ (TSS)\left(mg\ \ L^{-1}\right)} \tag{1}$$

SVI measurements were not possible for Site 1 CaO stage 2 and Site 2 stage 2 NaOH due to sampling errors. Total suspended solids (TSS) were performed according to Standard Methods (Franson and Eaton, 2005). 10 mL of the separated sludge was centrifuged (Eppendorf Centrifuge 5810) for 5 min at 3200 rcf with the sludge height measured afterwards reflecting the theoretical minimal sludge volume.

To test the differences in drying time and to determine the theoretical minimal sludge volume, 50 mL of each sludge was weighed, they were simultaneously dried in an oven at 60–70°C and weighed regularly until the weight recorded a constant value. Linear regression using Microsoft Excel 2016 was performed during the 70 °C period (23.5 h until the end of drying time) to identify any differences in sludge drying time by comparing the 95% confidence intervals of the slope parameter (Ryan, 2007). The dried solids from the sludge were analysed for their bulk chemical composition using ICP-OES and ICP-MS.

The next stage of the electrochemical treatment was identical to the first, except the pH was now elevated to the maximum attainable. There is a maximum pH that will be reached as, due to the cell configuration and type of membrane being used, hydroxide ion migration will begin to dominate the ion transport across the AEM (Thompson Brewster et al., 2017). The hydroxide migration reduces the amount of sulfate being removed from the cathode side until steady state conditions are reached. Observation under the experimental conditions indicated a maximum pH of ~10.2 could be reached. After the pH reached ~10.2, the current was again turned off and the same methods as above were repeated.

2.2.6. Direct comparison with chemical dosing approaches

To directly compare the electrochemical treatment performance with commonly used chemical precipitation, the same experiments were performed with AMD from Sites 1 and 2, except rather than using a cathode for pH adjustment, neutralisation was achieved via chemical addition of NaOH (Merck Pty Ltd, pellets for analysis, CAS-No: 1310-73-2) or slaked lime (Alfa Aesar, reagent grade, CAS-No: 1305-78-8). These tests were performed with the AMD contained in a beaker under constant magnetic stirring. In the same order as for the electrochemical experiments, the pH was adjusted to 4.2, then the same series of settling and sludge tests were performed. Subsequently, the solid and liquid phases separated, and the liquid was supplied with further additions of NaOH or lime until pH 10.2, where the same settling and sludge tests performed. The lime was prepared by mixing 1 part CaO with 9 parts MilliQ water and stirring at a high rate on a magnetic stirrer for at least 10 min prior to use. Due to the relative lack of solubility of CaO and its difficulty to handle when dry, lime is hydrated in this way during industrial use.

2.2.7. Multistage tests

The multistage tests were performed similar to the electrochemical two-stage tests, but with an increased number of steps at pH values of 3, 3.5, 4, 4.5, 5, 6, 7, 8, 9, 10 and the maximum possible value (~10.2). 1 L of Site 2 AMD was used and 0.5 L Site 1 AMD was used as catholyte solutions in the experiments, these were not replenished. The anolyte was 200 mL 0.5 M sodium borate buffer solution. These were replaced if necessary when the anolyte pH fell below 7. After each pH increment was reached, the reactor was stopped, emptied and the liquid left to settle for at least 1 h. After this, 10 mL or 4 mL samples were taken from Site 2 and Site 1 experiments, respectively. The liquid was decanted from the sludge. The liquid was used in the next stage. The remaining sludge was dried at 65 °C with the mass of sludge and solids percentage evaluated. The dried solids from the sludge were analysed for their bulk chemical composition using ICP-OES and ICP-MS.

3. Results & discussion

3.1. Modelling results and aqueous phase removal

3.1.1. Precipitation of solids

Graphs of the model output for the precipitants are available in the ESI Figs. S2–S3 (formation of dominant metal precipitants when Sites 1 and 2 AMD undergoes continuous electrochemical sulfate removal, chemical lime addition and chemical sodium hydroxide addition). All results clearly show that, as the pH increases, the precipitation of Al occurs firstly as jurbanite ($AlOHSO_4$) and then as diaspore ($AlOOH$). Buffering occurs at pH 4 while diaspore is forming. Once Al is completely depleted from the aqueous phase, the pH rises again until a second plateau. The second buffering stage occurs at ~ pH 10, where brucite ($Mg(OH)_2$) formations absorbs additional alkalinity produced by the treatment. Consistent results were observed for the three types of treatment, indicating this is a trend common to AMD containing high concentrations of Al and Mg. The modelling and experimental results illustrate that metals are not removed from solution evenly with increasing pH, and these differences can be used to target desirable compositions of the solid precipitants. It also illustrates that the trend in removal for the major metals is effectively independent from the type of treatment – chemical or electrochemical.

3.1.2. Removal of metals from the liquid phase

Fig. 1 shows that the electrochemical system removes iron, aluminium, magnesium and sulfate, while levels of sodium and calcium remain constant. The model of Site 1 does not accurately model sulfate, magnesium and aluminium. Epsomite ($MgSO_4$) was included in the PHREEQC model, but it does not reach saturation there. However, it is clearly forming experimentally based on the discrepancy between the experimental and model results for magnesium and sulfate. As the concentration of magnesium is over 6 times higher in Site 1 compared to Site 2, the discrepancy is exacerbated there. It is also possible that for both Site 1 and Site 2, jurbanite ($AlOHSO_4$) is not initially saturated, as the model predicts, which explains the slower than predicted removal of aluminium during the experiment at the lower pH (Thompson-Brewster et al., 2018).

The modelling results illustrate two key findings: i) there is more complexity occurring in the experiment than is reflected in the model; and ii) there is room to improve the modelling of AMD treatments. The model-practice differences could be due to:

- Inaccurate chemical databases (Parkhurst et al., 2013);

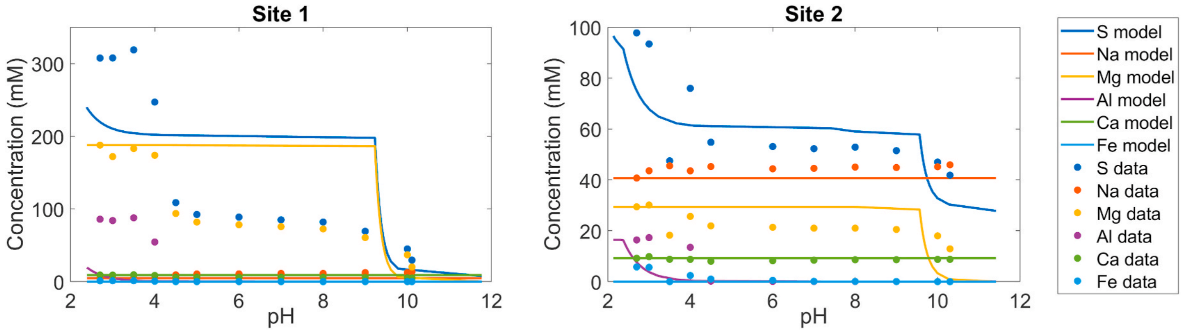

Fig. 1. Experimental (markers) and modelled (lines) contaminants in the liquid phase during electrochemical treatment of acid mine drainage (chemicals listed are their total components).

- Complex solutions with high ionic strength requiring a model accounting for more complex activity correlations (Parkhurst et al., 2013; Thompson Brewster et al., 2017); and/or
- Lack of inclusion of all lower concentration metals in the simulations.

Modelled data of the two stage experiments were compared to the experimental data (Tables S4 and S5 of the ESI). Despite the inaccuracies described above, the modelling results illustrate the usefulness of PHREEQC to indicate whether a solid is likely to form at stage 1 (<pH 4.2) or stage 2 (pH 4.2–10.2). Modelling of the NaOH and lime chemical treatment was also performed across the whole pH range (ESI Figs. S4–S5). In comparison to the NaOH and lime treatment, electrochemical treatment is expected to have lower concentrations of Ca compared to CaO dosing, and lower concentrations of Na and S compared to NaOH dosing. NaOH addition is not expected to reduce the sulfate concentrations and increases the Na concentration. However, NaOH treatment does remove Fe, Al and Mg successfully. Lime addition displays similar removal efficacy compared to ECR treatment. However, towards the high end of the pH range Ca concentrations in the liquid phase increase. This comparison is continued in Section 3.2.

3.2. Water discharge characteristics

3.2.1. Treated AMD characteristics – liquid fraction

Table 1 provides data for the final water quality of the AMD compared to two potential downstream uses as set out by the Australian and New Zealand Environment and Conservation Council and Agriculture and Resource Management Council of Australia and New Zealand (ANZECC and ARMCANZ) (2000). For both Site 2 and Site 1 AMD, all 3 treatment options removed nearly all listed contaminants to meet these guidelines, except for sulfate and manganese. Another exception was during lime treatment, in which there was insufficient removal of Al in Site 2 and Pb in Site 1. For Site 2, the lime treatment removed 23–26% more sulfate compared to electrochemical treatment. For Site 1, ECR treatment removed the most sulfate by approximately 14–25% compared to lime. In both cases, NaOH chemical treatment did not considerably diminish the sulfate concentration. Lime and electrochemical treatment were similar overall. However, lime treatment had two exceptions in meeting the discharge guidelines.

Sulfate levels from all the experiments did not meet discharge guidelines. It is likely that with further work an improved electrochemical configuration (e.g. different membrane type, current density, flow rate and/or chamber size) could improve sulfate removal during electrochemical treatment. For sensitive receiving waters, the electrochemical treatment could be combined with further biological polishing or dilution to meet discharge standards.

Some elements are potentially relevant to the ANZECC guidelines (2000), but are not included in the table as they were not detected in the ICP-OES analysis, which was performed on the liquid fraction (see Table 1 footnotes). The ICP-MS results of the solid precipitate showed at least partial, if not full removal of arsenic, beryllium, molybdenum, selenium, uranium and vanadium was achieved for all 3 treatment types (data not shown). Mercury was below the detection limit of the ICP-MS in all the samples and fluoride was not measured. These metals are of significant toxicity and further work demonstrating effective removal to below guideline values is recommended.

3.3. Precipitated solids

3.3.1. Removal of metals from solution

The multistage experiments illustrate that all the metals fall into three removal clusters when treated using the ECR: removal at low pH, high pH and continuously removed. Fig. 2 shows that Al, Ba, Cr, Cu, Fe and Pb precipitate at low pH (blue). Mg and Mn at high pH (green) and Cd, Co, Ni and Zn are removed continuously (red). The results from Site 2 AMD clearly show this trend. However, for Site 1 many metals are shown to precipitate at relatively low pH. This could be explained by the very high concentrations of SO_4^{2-} and Mg in Site 1 AMD (29 000 mg SO_4^{2-} L^{-1}, 4500 mgMg L^{-1}) which with both alter the ionic strength of the solution and require a large amount of current to be applied (i.e. the concomitant addition of OH^- and migration of SO_4^{2-}) before the pH increases significantly.

This order of sequential precipitation is further supported by the two stage experiments where Al, As, Ba, Cr, Cu, Fe, Mo, Se, Pb are mostly removed during the first stage; Co, Mg, Mn, Ni, Zn are largely removed during the second stage and Cd is removed in both stages relatively equally (ESI Figs. S6–S9 for supporting data).

3.3.2. Sludge composition

Fig. 3 shows the variation in sludge composition at the different pH stages. These graphs clearly illustrate the possibility of producing solid products with targeted composition dependent on the pH stage. The variation in bar colour highlights the precipitation of Fe, Al, Zn, Mg and Mn with increasing pH stages. Differences in staged composition are largely dependent on the initial composition of the AMD. The general trends between the results in Fig. 3 as well as the modelling above support the selective precipitation of Fe ($pH < 4$), Al (pH 4–6) then Mg and Mn ($pH > 7$) as the highest concentration metals in the solid product. This data supports the findings in Section 3.1 and illustrates that the experimental results follow closely the solubility models and associated theory for the higher concentration metals.

Seo et al. (2017) observed precipitation of Al between pH 3.5–5.5, Fe between pH 3.5–7.5 and Mn at pH 7.5–9.5 when performing chemical neutralisation using NaOH, $Ca(OH)_2$ or Na_2CO_3 to real coal mine tailings. It was observed that Al and Fe co-precipitated, but improved separation of Al and Fe was achieved when hydrogen peroxide was added initially to oxidise the Fe(II) to Fe(III). After oxidation, the majority of Fe precipitated at a lower pH to Al and could be separated and this result is similar to that seen in the Site 2 results in Fig. 3. While assessment of the

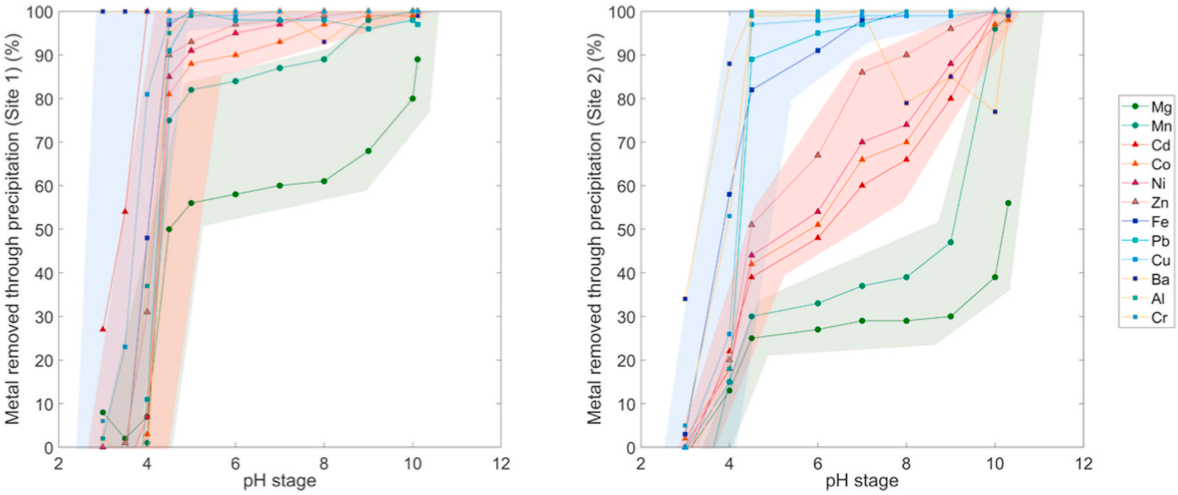

Fig. 2. Percentage removal of metals from acid mine drainage through electrochemically induced precipitation. Pollutants removed at low pH are indicated by blue square markers (also shaded blue), those removed at high pH by green circle markers (shaded green) and those constantly removed by red triangle markers (shaded red). The three classes of results and not clearly seen in the Site 1 results due to the very high concentrations of SO_4^{2-} and Mg, dominating the results (29 000 mg SO_4^{2-} L^{-1}, 4500 mg Mg L^{-1}). Chemicals listed are their total components not individual species. (For interpretation of the references to colour in this figure legend, the reader is referred to the Web version of this article.)

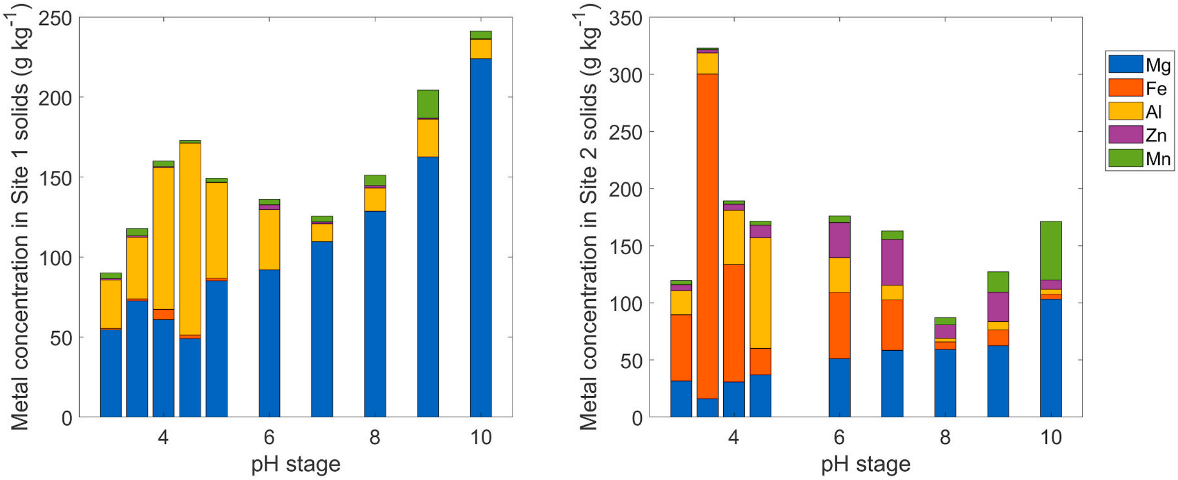

Fig. 3. Solids composition of key major metals at increasing pH stages. Left: results from the treatment of AMD from Site 1. Right: results from the treatment of AMD from Site 2. Chemicals listed are their total components not individual species.

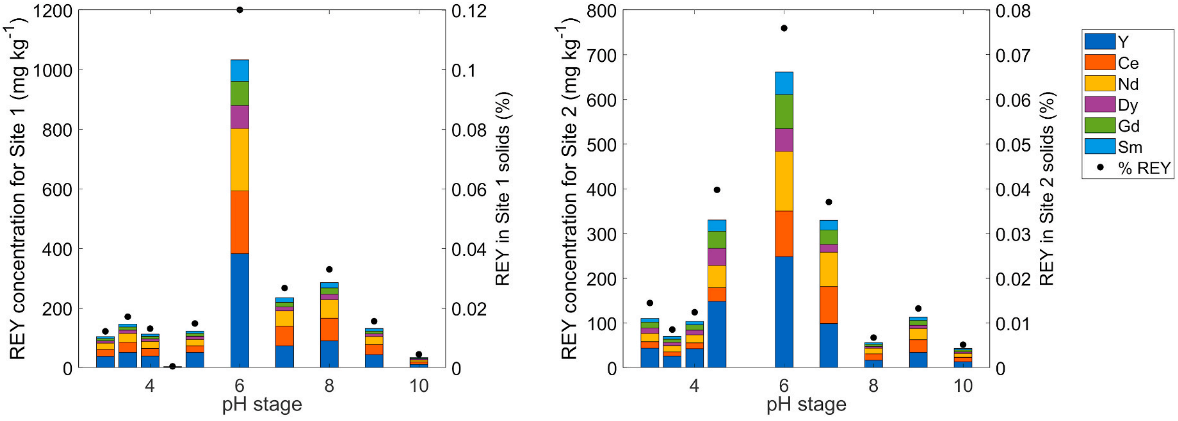

Fig. 4. Solids composition of rare earth element oxides at varying pH stages. The gap between the presented REYs and the total percentage is comprised of Erbium (Er), Europium (Eu), Holmium (Ho), Lutetium (Lu), Praseodymium (Pr), Terbium (Tb), Thulium (Tm) and Ytterbium (Yb). Left: results from the treatment of AMD from Site 1. Right: results from Site 2. Chemicals listed are their total components, not individual species.

Fe oxidation state was not performed, it is likely that it was mainly Fe (III) as the majority of Fe precipitated at a lower pH to Al.

3.3.3. Recovery of rare earth elements

The percentage of rare earth elements and yttrium (REYs) in the solids are shown in Fig. 4. The highest concentration REYs are Yttrium (Y), Neodymium (Nd), Cerium (Ce), Gadolinium (Gd), Dysprosium (Dy) and Samarium (Sm). Also detected in lower concentrations were Erbium (Er), Europium (Eu), Holmium (Ho), Lutetium (Lu), Praseodymium (Pr), Terbium (Tb), Thulium (Tm) and Ytterbium (Yb). Fig. 4 illustrates the maximum concentrations of REYs occur between a specific pH of 5–7 and is consistent between the two types of AMD.

Table 2 shows the values from that previous work compared to the values observed herein. The values in Pozo et al. (2017) are generally higher than observed, even at pH 6. However, they are in a similar order of magnitude (variations can be explained by seasonal changes in AMD due to e.g. rainfall).

3.3.4. Comparison to chemical dosing

3.3.4.1. Major metal composition. In the dried solids, metals recovered during the chemical experiments were found in lower concentrations compared to metals in the electrochemical experiments. This effect is due to the additional Ca and Na, which were precipitating during the chemical experiments, effectively 'diluting' the metal concentrations in the solid product. Our results support our previous findings (Pozo et al., 2017) indicating that an electricity-driven process can increase the concentration of metals compared to conventional chemical addition processes. See Figs. S10 and S11 in the ESI for further details.

3.3.4.2. Rare earth element recovery. Fig. 5 compares the REY concentrations in electrochemically-and chemically-generated solids. Stage 2 (S2, between pH 4–10) is where the majority of REYs precipitate (see Fig. 4, Section 3.3.3). Of particular note, in all cases the electrochemically-generated solids have a higher REYs percentage composition compared to chemically-generated solids. Similarly, as described above in the discussion on major metals, the solids from the chemical addition treatments also contain a significant mass of the elements that were added.

3.3.4.3. Sludge characteristics. As found from the drying experiments described in Section 2.2.5, the theoretical minimal sludge volume per litre of AMD was at least halved for electrochemically-generated sludge for both samples (Supplementary Information Fig. S12). This is similar to the (bio)electrochemically-generated sludge from Pozo et al. (2017) which was half the volume when compared to sludge produced through NaOH chemical addition neutralised to the same pH of 7.3. Here, the electrochemically produced sludge was between 2 and 20 times smaller in volume compared to NaOH addition.

For all treatments, the electrochemically-generated sludge had the lowest SVI (Sludge Volume Index) of those measured. There was one exception for Site 2 CaO stage 1, which had a particularly low SVI, corresponding to a very fast settling sludge (See Figs. S13–S15). Again these results are similar to previous observations where an SVI for NaOH chemical addition was ~4 times greater than (bio)electrochemically produced sludge (Pozo et al., 2017). The SVI for electrochemically-generated sludge from Site 1 (S1 2.7 ± 0.1, S2 15.1 ± 0.5 mL g-1) and Site 2 (S1 68.1 ± 2.2, S2 46.5 ± 1.5 mL g^{-1}) are a similar order of magnitude to the 58 mL g^{-1} SVI than (bio)electrochemically-generated sludge (Pozo et al., 2017) but the reactor configuration in this work is simpler and easier to operate. In contrast, the SVI for sludge generated through NaOH addition was always larger (Site 2 S1 200 ± 30, Site 1 S1 14.9 ± 1.7 and S2 36.4 ± 3.4 mL g^{-1}), which is similar to Pozo et al. (2017) and the 217 mL g^{-1} observed by Djedidi et al. (2009) or the 377 mL g^{-1} measured by Herrera et al. (2007).

Table 2
REY concentrations in solids at pH 6 compared to previous REY recovery using a more complex microbial/electrochemical process; uncertainties represent total standard deviation from triplicate samples analysed (Agilent 7900 ICP-MS) (Pozo et al., 2017). Confidence intervals in the data from Site 1 and Site 2 represent the relative standard deviation (%) evaluated during the ICP-MS analysis (Agilent 8800 ICP-MS-QQQQ; see Table S2 in ESI).

Element	Pozo et al. (2017)	Site 1	Site 2
Y	498 ± 70	382.6 ± 1.8	248 ± 2
Nd	166 ± 27	209.0 ± 1.1	133 ± 2
Gd	155 ± 14	81 ± 3	76.5 ± 1.4
Dy	140 ± 26	77 ± 4	51.0 ± 1.5
Sm	85 ± 13	72 ± 4	50.1 ± 1.4
Ce	82 ± 15	210.4 ± 0.7	102 ± 3

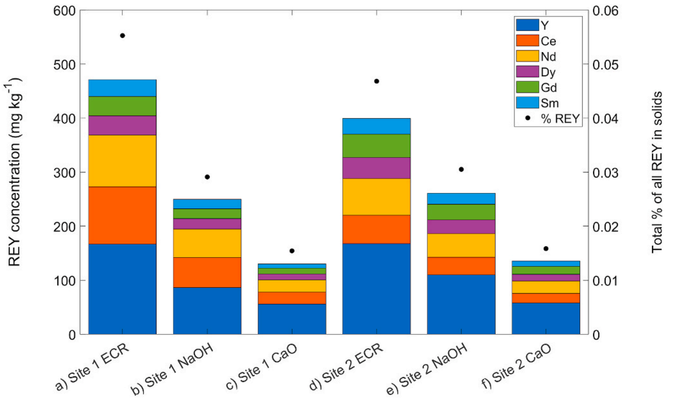

Fig. 5. Solids composition of REYs using electrochemical treatment and chemical (CaO and NaOH) addition. All values are for Stage 2 (pH 4–10), as this was the pH range where the majority of REYs were shown to precipitate.

For Site 1, stage 1 and stage 2 electrochemically-generated sludge (after settling, but before centrifugation) had the lowest percentage of solids by weight in the sludge (see Table S6). For Site 2, NaOH-created sludge had the lowest percentage of solids for both stages and CaO had the highest for both stages. Moreover, there were no significant differences in the time it took the different sludges to dry (Figs. S16–S17). For Site 1 there was only one sample that produced sufficient sludge for comparison. However, this dried faster than the other NaOH and lime-treated samples for Site 1. This provides some evidence that the electrochemically-generated sludge may dry faster in terms of its dewaterability, but this requires further investigation to confirm.

3.4. Preliminary OPEX analysis of electrochemical treatment vs conventional lime-dosing approach for AMD neutralisation

The two-stage experiments (see **2.2.5**) were used to compare the operational expenditure costs (OPEX) of the proposed electrochemical treatment system *versus* the conventional practice of lime-dosing to fully neutralise AMD to pH 10.2. Chemical-dosing costs were established based amount of lime added per litre of AMD, while the OPEX for electrochemical treatment were based on power consumption (calculated assuming a constant 8 V at 0.3 A, a conservative average value significantly overestimated compared to a fit-for-purpose reactor design at pilot- or even full-scale). When comparing treatment costs however, it is worth noting that a well-established figure for OPEX + CAPEX (capital expenditure) for the treatment of AMD in legacy mines is known to be approximately $100 AUD kL^{-1} irrespective of applied technology, given that site expenditure is predominantly driven by transport costs (mainly equipment + chemicals) and electricity use (Wang et al., 2018).

Based on bulk Queensland (Australia) electricity prices of $76.92 AUD MWh^{-1} (BulkEnergy, 2018), the conservative OPEX of the proposed electrochemical AMD treatment costs for Site 1 and Site 2 would be $1.6 and $5.2 AUD kL^{-1} respectively. The costs of lime in contrast –

based also on a conservative bulk price of \$100 AUD ton^{-1} (Millford&Company, 2018) – would result in a lower OPEX of \$0.48 and \$1.5 AUD kL^{-1} for Site 1 and 2 respectively (not considering the cost of water at a 9:1 ratio vs lime required for hydrating the lime, a process known as "slaking", which requires energy-intensive mixing and clean water to convert dry Lime CaO to its reactive hydrated form $Ca(OH)_2$). While apparently distant, the difference in these numbers is statistically insignificant with regards to the ~\$100 AUD kL^{-1} OPEX + CAPEX of AMD remediation. These relatively-small differences in \$ kL^{-1} *versus* lime-dosing could be easily overcome by demonstrating the value of: *(i)* the lower-volume/more-easily-settleable-sludge production, *(ii)* the significant water savings by eliminate slaking needs, and *(iii)* the possibility to selectively recover metals and REY using pH-driven staged precipitation. Further site-specific research is needed however to determine the actual value of these benefits through upcoming pilot-scale studies in 2020.

3.5. *Considerations for scaling-up the process and future work*

While the mining and environmental sectors are generally sceptical about electrochemical technologies, it is worth keeping in mind that many industrial electrochemical-cell-based processes have operated successfully for decades, with the high CAPEX offset by low OPEX, even if the product is low value. For example, the chlor-alkali process is able to meet the global demand for relatively-low value caustic (Strathmann, 2004). As in the latter, up-scaling of our process will be achieved by manufacturing a stack of litre-scale electrochemical cells that will allow for a more detailed and long-term CAPEX/OPEX analysis including energy and mainstream/REY metal recovery efficiencies for site-specific conditions and AMD compositions and comparison with other technologies within the context of a circular economy (Du et al., 2018). Our recent research has demonstrated that the electrochemical stacking strategy is able to maintain up-scaled cell voltages close to laboratory values (Ledezma et al., 2019; Ward et al., 2018), meaning that a pilot-scale version of the system hereby proposed can be easily powered by off-grid solutions (*e.g.* generator, solar PV) ideally suited to remote or legacy mine sites. Long-term operation will also reveal details over predictable problems such as material wear/tear and electrode scaling. The latter was observed at the cathode in this study – due to the inevitable formation of Fe/Ca/Mg (oxy)hydroxide precipitates at high pH – but did not observably affect the performance of the system during the testing period (data not shown). Longer-term operation will reveal the rate of this scaling and allow for the determination of a de-scaling regime which can be undertaken without any chemical dosing by: i) periodically utilising the sulfuric acid formed in the anodic chamber as a de-scaling agent and/or ii) switching off the current and allowing for the cathode chamber to be filled with fresh AMD. The resulting strong acidification dissolves the (oxy)hydroxides and regenerates the electrode surface – as we have previously observed in the laboratory (Pozo et al., 2017) but only with pilot-scale testing can the frequency and extent of this cleaning regime be determined and subsequently automated as part of a fully-autonomous decentralised process control system.

CRediT authorship contribution statement

Emma Thompson Brewster: Conceptualization, Methodology, Software, Formal analysis, Writing - original draft, Writing - review & editing. **Stefano Freguia:** Methodology. **Mansour Edraki:** Supervision, Methodology, Data curation, Project administration, Funding acquisition. **Luke Berry:** Project administration, Funding acquisition. **Pablo Ledezma:** Conceptualization, Methodology, Resources, Supervision, Writing - review & editing.

Declaration of Competing interest

The authors declare the following financial interests/personal relationships which may be considered as potential competing interests: The authors declare that E.T. Brewster and L. Berry contributed to this study while employed by Kinetic Group Worldwide Pty Ltd, who has filed a provisional patent for the proposed technology with intent to commercialise.

Acknowledgements

The authors thank the Queensland Government for supporting Dr Emma Thompson Brewster through a Knowledge Transfer Partnership Grant. Dr Pablo Ledezma acknowledges a Development Fellowship from The University of Queensland. The authors furthermore acknowledge the services provided by the Analytical Services Laboratory at The University of Queensland (Dr Beatrice Keller-Lehmann and Mr Nathan Clayton), the Central Analytical Research Facility at Queensland University of Technology (Dr Sunny Hu and Dr Sam Ghidan) and ALS Global. The Queensland Government's Department of Natural Resources, Mines & Energy (DNRME) provided the field collected AMD samples, and the authors acknowledge that the extent of their support was simply to provide the samples with no implication of endorsement of the sampling results or the treatment methodologies as presented here.

Appendix A. Supplementary data

Supplementary data to this article can be found online at https://doi.org/10.1016/j.jenvman.2020.111266.

References

Akcil, A., Koldas, S., 2006. Acid Mine Drainage (AMD): causes, treatment and case studies. J. Clean. Prod. 14, 1139–1145.

Alonso, E., Sherman, A.M., Wallington, T.J., Everson, M.P., Field, F.R., Roth, R., Kirchain, R.E., 2012. Evaluating rare earth element availability: a case with revolutionary demand from clean technologies. Environ. Sci. Technol. 46, 3406–3414.

Arshi, P.S., Vahidi, E., Zhao, F., 2018. Behind the scenes of clean energy: the environmental footprint of rare earth products. ACS Sustain. Chem. Eng. 6, 3311–3320.

Barnhart, C.J., Benson, S.M., 2013. On the importance of reducing the energetic and material demands of electrical energy storage. Energy Environ. Sci. 6, 1083–1092.

Bejan, D., Bunce, N.J., 2015. Acid mine drainage: electrochemical approaches to prevention and remediation of acidity and toxic metals. J. Appl. Electrochem. 45, 1239–1254.

Browne, M.P., Sofer, Z., Pumera, M., 2019. Layered and two dimensional metal oxides for electrochemical energy conversion. Energy Environ. Sci. 12, 41–58.

BulkEnergy, 2018. Australian Electricity Prices; the Cost of Electricity in Australia Per kWh.

Chartrand, M.M.G., Bunce, N.J., 2003. Electrochemical remediation of acid mine drainage. J. Appl. Electrochem. 33, 259–264.

Djedidi, Z., Médard, B., Cheikh, R.B., Mercier, G., Tyagi, R.D., Blais, J.-F., 2009. Comparative study of dewatering characteristics of metal precipitates generated during treatment synthetic polymetallic and AMD solutions. Hydrometallurgy 98, 247–256.

DNRME, Q.G., 2018. Abandoned Mines Remediation Projects: Mount Morgan Mine.

Du, F., Warsinger, D.M., Urmi, T.I., Thiel, G.P., Kumar, A., Lienhard, V.J.H., 2018. Sodium hydroxide production from seawater desalination brine: process design and energy efficiency. Environ. Sci. Technol. 52, 5949–5958.

Fernando, W.A.M., Ilankoon, I.M.S.K., Syed, T.H., Yellishetty, M., 2018. Challenges and opportunities in the removal of sulphate ions in contaminated mine water: a review. Miner. Eng. 117, 74–90.

Franson, M.A.H., Eaton, A.D., 2005. Standard methods for the examination of water & wastewater. In: Eaton, Andrew D., et al. (Eds.), Centennial Ed./Prepared and Published Jointly by American Public Health Association, American Water Works Association, Water Environment Federation Joint Editorial Board, twenty-first ed. American Public Health Association, Washington, DC. Mary Ann H. Franson.

Herrera, S.P., Uchiyama, H., Igarashi, T., Asakura, K., Ochi, Y., Ishizuka, F., Kawada, S., 2007. Acid mine drainage treatment through a two-step neutralization ferrite-formation process in northern Japan: physical and chemical characterization of the sludge. Miner. Eng. 20, 1309–1314.

Kefeni, K.K., Msagati, T.A.M., Mamba, B.B., 2017. Acid mine drainage: prevention, treatment options, and resource recovery: a review. J. Clean. Prod. 151, 475–493.

Ledezma, P., Monetti, J., Virdis, B., Freguia, S., 2019. Successful pilot up-scaling, decentralisation and automation of a microbial electrochemical system for nutrient recovery from source-separated urine. In: 16th IWA Leading Edge Conference on Water and Wastewater Technologies. International Water Association, Edinburgh, U. K.

Millford&Company, J.R., 2018. ChemLink Index of Chemicals in Australia.

Morel, F.o., Hering, J.G., Morel, F.o., 1993. Principles and Applications of Aquatic Chemistry. Wiley, New York.

Naidu, G., Ryu, S., Thiruvenkatachari, R., Choi, Y., Jeong, S., Vigneswaran, S., 2019. A critical review on remediation, reuse, and resource recovery from acid mine drainage. Environ. Pollut. 247, 1110–1124. https://doi.org/10.1016/j.envpol.2019.01.085.

Nleya, Y., Simate, G.S., Ndlovu, S., 2016. Sustainability assessment of the recovery and utilisation of acid from acid mine drainage. J. Clean. Prod. 113, 17–27.

Parkhurst, D.L., Appelo, C.A.J., Geological, S., 2013. Description of input and examples for PHREEQC version 3–a computer program for speciation, batch-reaction, one-dimensional transport, and inverse geochemical calculations.

Pozo, G., Pongy, S., Keller, J., Ledezma, P., Freguia, S., 2017. A novel bioelectrochemical system for chemical-free permanent treatment of acid mine drainage. Water Res. 126, 411–420.

Rakotonimaro, T.V., Neculita, C.M., Bussière, B., Zagury, G.J., 2016. Effectiveness of various dispersed alkaline substrates for the pre-treatment of ferriferous acid mine drainage. Appl. Geochem. 73, 13–23.

Ryan, T.P., 2007. Modern Engineering Statistics. Wiley-Interscience John Wiley, Hoboken, N.J. Hoboken, NJ.

Seo, E.Y., Cheong, Y.W., Yim, G.J., Min, K.W., Geroni, J.N., 2017. Recovery of Fe, Al and Mn in acid coal mine drainage by sequential selective precipitation with control of pH. CATENA 148, 11–16.

Simate, G.S., Ndlovu, S., 2014. Acid mine drainage: challenges and opportunities. J. Chem. Environ. Eng. 2, 1785–1803.

Strathmann, H., 2004. Ion-exchange Membrane Separation Processes, first ed. Elsevier, Amsterdam ; Boston.

Stumm, W., Morgan, J.J., 2013. Aquatic Chemistry: Chemical Equilibria and Rates in Natural Waters, third ed. John Wiley & Sons Inc.

Thompson-Brewster, E., Pozo, G., Batstone, D.J., Freguia, S., Ledezma, P., 2018. A modelling approach to assess the long-term stability of a novel microbial/electrochemical system for the treatment of acid mine drainage. RSC Adv. 8, 18682–18689.

Thompson Brewster, E., Jermakka, J., Freguia, S., Batstone, D.J., 2017. Modelling recovery of ammonium from urine by electro-concentration in a 3-chamber cell. Water Res. 124, 210–218.

Thompson Brewster, E., Mehta, C.M., Radjenovic, J., Batstone, D.J., 2016. A mechanistic model for electrochemical nutrient recovery systems. Water Res. 94, 176–186.

van Loosdrecht, M.C.M., Nielsen, P.H., Lopez-Vazquez, C.M., Brdjanovic, D., 2016. Experimental Methods in Wastewater Treatment, 1 ed. Iwa Publishing.

Wang, Y., Tavakkoli, S., Khanna, V., Vidic, R.D., Gilbertson, L.M., 2018. Life cycle impact and benefit tradeoffs of a produced water and abandoned mine drainage Co-treatment process. Environ. Sci. Technol. 52 (23), 13995–14005. https://doi.org/10.1021/acs.est.8b03773.

Ward, A.J., Arola, K., Thompson Brewster, E., Mehta, C.M., Batstone, D.J., 2018. Nutrient recovery from wastewater through pilot scale electrodialysis. Water Res. 135, 57–65.

Zealand, A.R.M., 2000. Australian and New Zealand Guidelines for Fresh and Marine Water Quality. Australian and New Zealand Environment and Conservation Council and Agriculture and Resource Management Council of Australia and New Zealand, Canberra, ACT.